Journal of Applied Physics ARTICLE pubs.aip.org/aip/jap

Recombination velocities at grain boundaries in solar-cell absorbers—Revisited

Cite as: J. Appl. Phys. **137**, 233106 (2025); doi: 10.1063/5.0274267
Submitted: 4 April 2025 · Accepted: 28 May 2025 ·
Published Online: 20 June 2025

View Online Export Citation CrossMark

Daniel Abou-Ras[1,a)] and Matthias Maiberg[2]

AFFILIATIONS

[1]Helmholtz-Zentrum Berlin für Materialien und Energie GmbH, Berlin,Germany
[2]Institute of Physics, Martin Luther University Halle-Wittenberg, Von-Danckelmann-Platz 3, 06120 Halle (Saale), Germany

[a)]**Author to whom correspondence should be addressed:** daniel.abou-ras@helmholtz-berlin.de

ABSTRACT

The present work revisits the recombination velocities (s_{GB}) of minority-charge carriers determined at grain boundaries in polycrystalline absorber materials for solar cells. The equations describing s_{GB} as well as the barriers for electrons and holes were derived. It is shown that for given net-doping density and absolute temperature, the experimentally determined recombination velocity of a specific grain boundary can be described by $s_{GB} = s^n_{GB,0} \exp\left[-\Phi_{GB}(N_{GB,charge})/(k_B T)\right]$, where Φ_{GB} is the band bending induced by the excess-charge density $N_{GB,charge}$ at the grain boundary, and k_B as well as T are the Boltzmann constant and the absolute temperature; i.e., s_{GB} depends only on the excess-charge density at this planar defect as well as on the prefactor $s^n_{GB,0}$ describing the nonradiative recombination. Value ranges for these two quantities can be determined for any measured s_{GB} value. When analyzing s_{GB} datasets acquired on various (Ag,Cu)(In,Ga)Se_2 and microcrystalline Si absorbers, it is apparent that both the excess-charge density and the prefactor $s^n_{GB,0}$ remain within about the same orders of magnitude for all grain boundaries analyzed in a specific absorber. The broad range of the recombination velocities over several orders of magnitude indicates upward as well as downward band bending, and the band-bending values are on the order of several ± 10 meV for all materials analyzed.

22 June 2025 06:41:20

© 2025 Author(s). All article content, except where otherwise noted, is licensed under a Creative Commons Attribution (CC BY) license (https://creativecommons.org/licenses/by/4.0/). https://doi.org/10.1063/5.0274267

I. INTRODUCTION

In the photovoltaic solar cells appropriate for low-cost production at high conversion efficiencies, most of the solar absorbers, with the exception of monocrystalline, wafer-based Si, are polycrystalline. Therefore, grain boundaries are present at densities corresponding to the average grain sizes in these absorbers. Since the (two-dimensional, projected) density of point defects at a grain-boundary plane is enhanced with respect to those (three-dimensional) in the grain interiors of the adjacent grains, the nonradiative recombination rate is enhanced and contributes to a corresponding loss in the open-circuit voltage of the solar cell. The quantification of the grain-boundary recombination via the recombination velocity s_{GB} and the effects on the device performance have been revised recently.[1] It was clarified that s_{GB} can be expressed by a prefactor containing an effective defect density at the grain boundary and its capture cross section multiplied by an exponential function depending on the band bending at the grain-boundary plane.

However, for the case of a grain-boundary plane as opposed to for a surface, the derivation for an equation describing the recombination velocity s_{GB} has not yet been published; we note that charge-carrier recombination at a grain-boundary plane may differ substantially from that at a surface plane in a specific material since the density of states for free charge carriers at a grain-boundary plane, and therefore, the recombination behaviors are influenced by the arrangement of two adjacent, and not just one adjacent, crystals. Moreover, the available literature (e.g., Ref. 2) provides equations only for the barriers of the majority charge-carriers at the grain boundary (i.e., upward/downward band bending for *n*-type/*p*-type semiconductors) and not for the accumulation of free electrons/holes at grain boundaries with a positive/negative excess charge in *n*-type/*p*-type semiconductors.

The present work first derived the equations of s_{GB} for low-injection and high-injection conditions. Also, the barriers of the majority charge-carriers at the grain boundary were calculated. It became apparent that the barriers for electrons or holes, provided

© Author(s) 2025

that the net-doping density is sufficiently high, depend for a given net-doping density and absolute temperature only on the excess-charge density at the grain boundary. It is highlighted that each s_{GB} value determined experimentally at a grain boundary can be simulated using appropriate values for the excess-charge density at the grain boundary and for the prefactor $s^n_{GB,0}$ describing the enhanced nonradiative recombination and that the ranges of these values remain within similar orders of magnitude for various photovoltaic absorber materials.

II. THEORY

A. Basic considerations

We assume a p-type semiconductor with net-doping density N_A. This also includes the case of a compensated, p-type semiconductor, for which the doping density is $N_a - N_d$ (i.e., the difference between the densities of an ionized acceptor and donor states). For this case, we write for the hole concentration in thermodynamic equilibrium: $p_0 = N_A = N_a - N_d$. Moreover, the electron density in the bulk under illumination is equal to the excess electron density: $n = n_0 + \Delta n \approx \Delta n$. The hole density in the bulk under illumination is equal to the sum of the net-doping density N_A and the excess electron density: $p = p_0 + \Delta p = N_A + \Delta n$, provided that charge carriers are not separated by strong internal electrical fields.

It is also assumed that under illumination, the quasi-Fermi levels are constant throughout the semiconductor. Then, at a grain-boundary plane, the electron and hole densities can be expressed by

$$n_{GB} = \Delta n \exp\left(-\Phi_{GB}/k_B T\right) \tag{1}$$

and

$$p_{GB} = (N_A + \Delta n) \exp\left(\Phi_{GB}/k_B T\right), \tag{2}$$

where Δn is the electron density at the edges of the space-charge regions at these planar defects, Φ_{GB} is the band bending at the grain-boundary plane (which either drives electrons/holes to or repels them from the grain boundary), k_B is the Boltzmann constant, and T the absolute temperature.

We consider the following scenario at the grain-boundary. In the case of a compensated, p-type semiconductor at room temperature, there are various positively charged donor and negatively charged acceptor states, in addition to neutral defect states. Each defect state exhibits a charge state (positive, negative, or neutral) and contributes to Shockley–Read–Hall (SRH) recombination. The present grain-boundary model simplifies this complex situation by assuming one effective defect state at a midgap position (since for such a defect, the SRH recombination is most effective) with density $N_{GB,recomb}$ and its capture cross sections for electrons and holes, σ_n and σ_p; and another effective defect state with density $N_{GB,charge}$ beyond the demarcation levels. This effective defect state exhibits an excess charge corresponding to whether the density of positively or that of negatively charged defect states at the grain boundary is larger (see Fig. 1).

Since the effective, charged defect density $N_{GB,charge}$ features a positive or negative excess charge, the free charge carriers redistribute correspondingly, i.e., leading to depletion or accumulation of these charge carriers around the grain boundary, provided that the net-doping density (N_A) is sufficiently large (Fig. 2). We note that for very small net-doping densities, the free charge carriers are captured by the defect state (trap); i.e., the grain interiors can be considered to be depleted of free charge carriers.[2] According to Poisson's equation, the redistribution of free charge carriers results in spatial variations in the electrostatic potential and thus in band bending. We note that for very large charge densities, theoretically, the upward band bending (p-type semiconductor) can take values of above the Fermi level; however, the grain-boundary model in the present work does not consider such a scenario.

B. Derivation of the equation for the recombination rate at a grain boundary

We use an equation describing the SRH recombination rate for an effective, deep defect level ($N_{GB,recomb}$); it is very similar to the one used for the SRH bulk recombination rate $R_{SRH} = \left(np - n_i^2\right)/\left(n\tau_p + p\tau_n\right)$ (τ_p and τ_n are the hole and electron lifetimes and n_i the intrinsic charge-carrier concentration). At a grain boundary, $n = n_{GB}$ and $p = p_{GB}$. Moreover, we assume $n_i^2 \ll np$. The recombination rate at the grain boundary can be expressed by

$$\begin{aligned} R_{GB} &= \frac{\Delta n \exp\left(-\Phi_{GB}/k_B T\right)(N_A + \Delta n) \exp\left(\Phi_{GB}/k_B T\right)}{\Delta n \exp\left(-\Phi_{GB}/k_B T\right)\left(s^p_{GB,0}\right)^{-1} + (N_A + \Delta n) \exp\left(\Phi_{GB}/k_B T\right)\left(s^n_{GB,0}\right)^{-1}} \\ &= \frac{\Delta n (N_A + \Delta n)}{\Delta n \exp\left(-\Phi_{GB}/k_B T\right)\left(s^p_{GB,0}\right)^{-1} + (N_A + \Delta n) \exp\left(\Phi_{GB}/k_B T\right)\left(s^n_{GB,0}\right)^{-1}}. \end{aligned} \tag{3}$$

Here, $s^p_{GB,0}$ and $s^n_{GB,0}$ are the recombination velocity parameters of holes and electrons at the grain boundary (we use expressions similar to those used at semiconductor surfaces[3]),

$$s^p_{GB,0} = N_{GB,recomb}\sigma_p v_{th} \tag{4}$$

and

$$s^n_{GB,0} = N_{GB,recomb}\sigma_n v_{th}, \tag{5}$$

where v_{th} is the thermal velocity of holes and of electrons (we assume that they are the same). Using Eqs. (4) and (5), Eq. (3) changes to

22 June 2025 06:41:20

© Author(s) 2025

$$R_{GB} = \frac{\Delta n(N_A + \Delta n)}{\Delta n \exp(-\Phi_{GB}/k_B T)(N_{GB,recomb}\sigma_p v_{th})^{-1} + (N_A + \Delta n)\exp(\Phi_{GB}/k_B T)(N_{GB,recomb}\sigma_n v_{th})^{-1}}$$
$$= \frac{\Delta n(N_A + \Delta n)N_{GB,recomb}v_{th}}{\Delta n \exp(-\Phi_{GB}/k_B T)\sigma_p^{-1} + (N_A + \Delta n)\exp(\Phi_{GB}/k_B T)\sigma_n^{-1}}$$
$$= \frac{\Delta n N_{GB,recomb}v_{th}}{[\Delta n/(N_A + \Delta n)]\exp(-\Phi_{GB}/k_B T)\sigma_p^{-1} + \exp(\Phi_{GB}/k_B T)\sigma_n^{-1}}. \quad (6)$$

C. Equations for the recombination velocity at a grain boundary

The following approach corresponds to the work by Brody and Rohatgi[4] who calculated the recombination velocity for a semiconductor surface. For a grain boundary, the effective recombination velocity is defined as

$$s_{GB} := \frac{R_{GB}}{\Delta n} = \frac{N_{GB,recomb}v_{th}}{[\Delta n/(N_A + \Delta n)]\exp(-\Phi_{GB}/k_B T)\sigma_p^{-1} + \exp(\Phi_{GB}/k_B T)\sigma_n^{-1}}. \quad (7)$$

We may consider two different injection conditions:

1. Low-injection condition

Here, we need to assume not only that $\Delta n \ll N_A$, but also that the downward band bending Φ_{GB} is not too strong; i.e., only if

$$\Delta n \ll N_A/\left[\exp(-2\Phi_{GB}/k_B T)\sigma_n/\sigma_p - 1\right], \quad (8)$$

then $\Delta n/(N_A + \Delta n)]\exp(-\Phi_{GB}/k_B T)\sigma_p^{-1} \approx 0$ in Eq. (7), and this equation becomes

$$s_{GB} = N_{GB,recomb}\sigma_n v_{th}\exp\left(-\frac{\Phi_{GB}}{k_B T}\right). \quad (9)$$

We note that in order for Eq. (8) to hold, Φ_{GB} for the downward band bending must remain small. For $\Phi_{GB} = -100$ meV and $\sigma_n/\sigma_p \approx 1$, the factor $\left[\exp(-2\Phi_{GB}/k_B T)\sigma_n/\sigma_p - 1\right]$ becomes about 3000. We consider $\Phi_{GB} = -100$ meV as a lower limit.

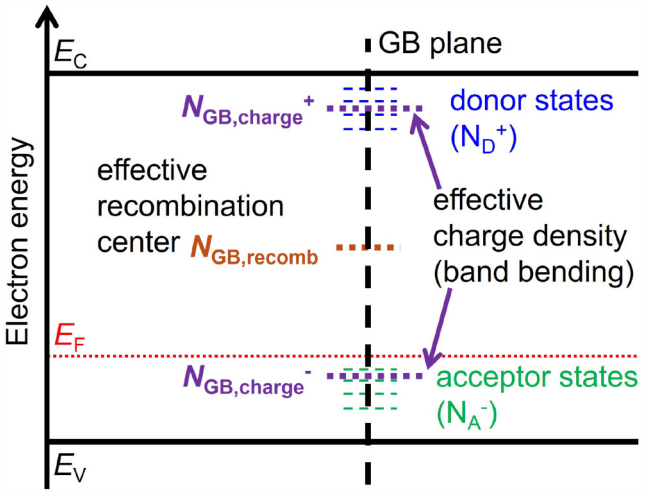

FIG. 1. Schematic equilibrium band diagram of a *p*-type semiconductor at room temperature around a grain-boundary (GB) plane. In the case of a compensated semiconductor, positively charged donor (N_D^+) as well as negatively charged acceptor states (N_A^-) are present, in addition to neutral defect states (not depicted here). The GB model in the present work assumes a simplified scenario with one effective defect density $N_{GB,recomb}$ at a midgap position for the SRH recombination and another effective defect density $N_{GB,charge}$, which can be positive or negative, depending on whether the density of positively or that of negatively charged defect states is larger. E_C, E_V, and E_F depict the conduction-band and valence-band edges as well as the Fermi level.

2. High-injection condition

$\Delta n \gg N_A$: $\Delta n/(N_A + \Delta n) \approx 1$.
Also, $\Phi_{GB} \approx 0$ since $n_{GB} \approx p_{GB}$

$$\Rightarrow s_{GB} = N_{GB,recomb}v_{th}\left(\sigma_p^{-1} + \sigma_n^{-1}\right)^{-1}. \quad (10)$$

D. The dependencies of Φ_{GB} and s_{GB} vs N_{GB} and σ_n

We note that for low-injection conditions, s_{GB} [Eq. (9)] is a function of $N_{GB,recomb}$ of σ_n and of Φ_{GB}. For downward band bending at the grain-boundary plane in a *p*-type semiconductor, Φ_{GB} is expressed by[2]

$$\Phi_{GB}^{down} = -\frac{\left(qN_{GB,charge}^+\right)^2}{8\epsilon_0\epsilon_r N_A}, \quad (11)$$

where ϵ_0 and ϵ_r are the dielectric permittivities of the vacuum and of the semiconductor (see also Sec. 2 in Appendix A). Note that

22 June 2025 06:41:20

© Author(s) 2025

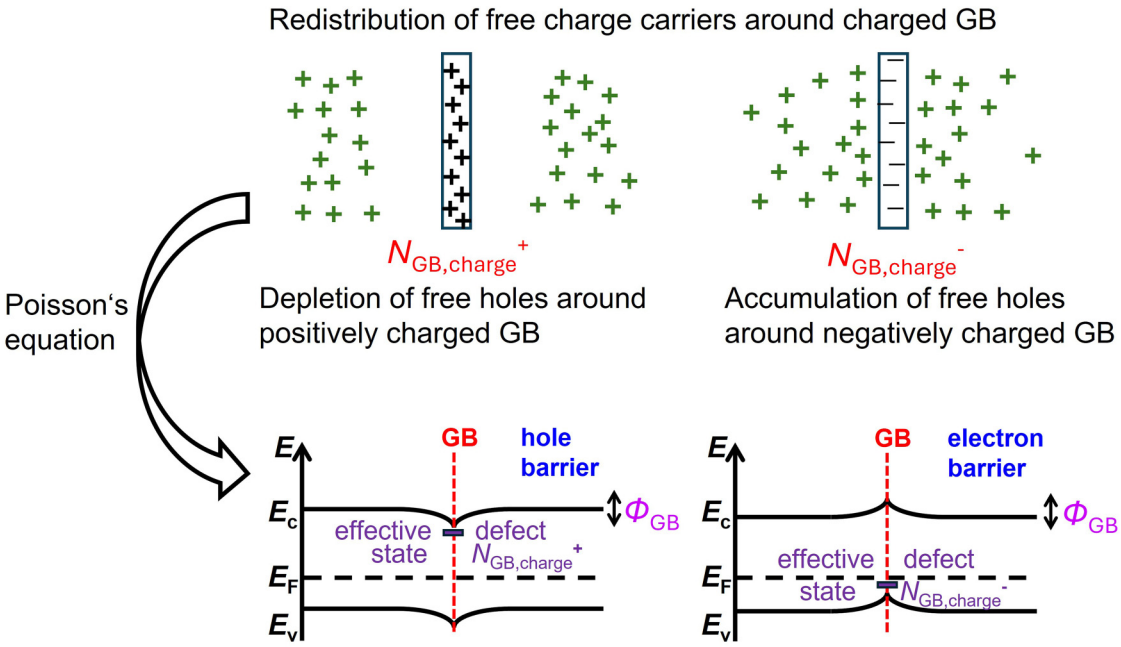

FIG. 2. Schematics depicting the origin of the band bending at a grain-boundary (GB) plane in a *p*-type semiconductor at room temperature. Free charge carriers (holes) redistribute correspondingly, provided that the net-doping density (p_0) is sufficiently large. According to Poisson's equation, the redistribution of free charge carriers results in downward (positive excess charge) or in upward band bending (negative excess charge).

22 June 2025 06:41:20

Eq. (11) is only valid for semiconductors that exhibit net-doping densities sufficiently large so that the trap states represented by the density of recombination centers $N_{GB,recomb}$ do not capture all free charge carriers, i.e., in case the grains in the polycrystalline semiconductor are only partly depleted.

The expression for the upward band bending is different (see Sec. 1 in Appendix A),

$$\Phi_{GB}^{up} = \frac{\sqrt{k_B T} q N_{GB,charge}^{-}}{4\sqrt{\epsilon_0 \epsilon_r N_A}}. \tag{12}$$

Note that for the derivation of (12), the Boltzmann approximation was used; thus, $\Phi_{GB}^{up} < E_F - E_V$, which is about 100–150 meV for net-doping densities N_A of about 10^{14}–10^{16} cm^{-3}. In the present work, we assume an upper limit for a Φ_{GB}^{up} of 100 meV.

It is convenient to rewrite Eq. (9) for low-injection conditions using Eqs. (4) and (5),

$$s_{GB} = s_{GB,0}^{n} \exp\left(-\frac{\Phi_{GB}(N_{GB,charge})}{k_B T}\right). \tag{13}$$

Thus, for given net-doping density N_A and absolute temperature T, Φ_{GB} is a function of $N_{GB,charge}$ and s_{GB} is a function of $N_{GB,charge}$ and $s_{GB,0}^{n}$. We can now vary both quantities within certain intervals and check the resulting value ranges for Φ_{GB} and s_{GB}. For the following considerations, we set $\epsilon_r = 12$ and $T = 300$ K. Corresponding to the considerations above, the current grain-boundary model is only valid for band-bending values Φ_{GB} within the interval of about −100 to +100 meV.

While in microcrystalline Si, the *p*-type net-doping density corresponds to the density of doping atoms (e.g., B for *p*-type Si), in compensated semiconductors, such as CdTe or $CuInSe_2$, the *p*-type conductivity is determined by a slight excess of acceptor over donor densities, which are both on the order of about 10^{17}–10^{19} cm^{-3}.[5–7] Assuming a grain-boundary width of <1 nm,[8] the density of net charges at the grain-boundary plane would result in about 10^{9}–10^{11} cm^{-2}. However, the general picture of a grain boundary is that it acts as a sink for point defects segregating during the growth from the grain interiors to these planar defects. Therefore, it is appropriate to assume a slightly larger range for $N_{GB,charge}$ of about 10^{9}–10^{12} cm^{-2}. Since for our model to be valid, Φ_{GB}^{down} and Φ_{GB}^{up} must not exceed $\mp$ 100 meV, there is an upper limit for $N_{GB,charge}$, which depends on the net-doping density N_A. Using Eqs. (11) and (12), the downward and upward band-bending values Φ_{GB}^{down} and Φ_{GB}^{up} were calculated for various net-doping densities N_A (see Fig. 3). Apparently, the upper limits for $N_{GB,charge}$, i.e., for which the corresponding downward (upward) band-bending values exceed $\mp$ 100 meV, are about 3×10^{10} (7×10^{10}), 6×10^{10} (2×10^{11}), 3×10^{11} (7×10^{11}), and 6×10^{11} (2×10^{12}) cm^{-2} for $N_A = 1 \times 10^{14}$, 1×10^{15}, 1×10^{16}, and 1×10^{17} cm^{-3}.

Assuming a net-doping density of $N_A = 2 \times 10^{16}$ cm^{-3}, s_{GB} values for downward and upward band bending were calculated

© Author(s) 2025

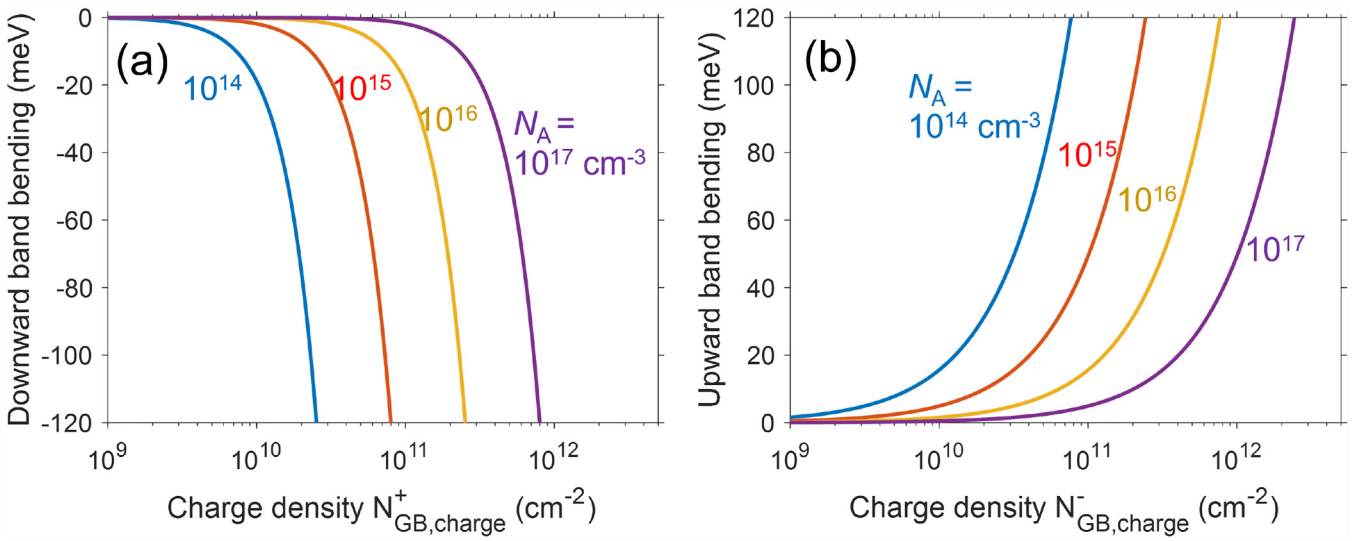

FIG. 3. (a) Downward band bending Φ_{GB}^{down} and (b) upward band bending Φ_{GB}^{up}, calculated as a function of the charged defect density $N_{GB,charge}$ for various net-doping densities N_A using Eqs. (11) and (12).

using Eq. (13). Since the experimentally determined s_{GB} values that are on the order of 10^0–10^4 cm/s,[9–12] the appropriate value range for $s^n_{GB,0}$ is about 10^{-1}–10^4 cm/s. In Fig. 4, we plotted the value range of s_{GB} as a function of the value ranges of $N_{GB,charge}$ and $s^n_{GB,0}$. We consider the upper limits for $N_{GB,charge}$ with respect to the downward and upward band bending mentioned above, 3×10^{11} and 9×10^{11} cm^{-2}. The lower limit of $N_{GB,charge}$ was set to 1×10^9 cm^{-2}.

From Fig. 4, it is clear that one specific s_{GB} value can be represented assuming a certain pair of $N_{GB,charge}$ and $s^n_{GB,0}$ values; and it is a range of appropriate values each that results in the same recombination velocity s_{GB}. Table I provides several ranges of s_{GB} values as well as the ranges of the corresponding $N_{GB,charge}$ and $s_{GB,0}$ values, assuming that they remain within the assumed intervals (0.01–3.3 or 0.01–9.1 $\times 10^{11}$ cm^{-2} and 1×10^{-1} to 1×10^5 cm/s).

E. Material-specific limits of $N_{GB,charge}$ and $s^n_{GB,0}$

While the results depicted in Table I are mathematically sound, the question is whether they can be confined to narrower intervals with respect to material properties in the solar-cell absorbers. In a polycrystalline semiconductor grown at elevated temperatures, the interdiffusion of constituting elements results in a rather homogeneous distribution of point defects, both in the bulk and at grain boundaries. Such a quasi-homogeneous distribution of point defects would lead to a corresponding distribution of effective defect densities $N_{GB,recomb}$ and their capture cross sections as well as of excess-charge densities at grain boundaries. Consequently, not identical, but similar values for $N_{GB,charge}$ and for $s^n_{GB,0}$ at different grain boundaries can be expected in the same polycrystalline absorber material. Thus, it is appropriate to assume that within a specific absorber material, the $N_{GB,charge}$ and $s^n_{GB,0}$ values remain within the same orders of magnitude.

As described above (Fig. 3), the band bending values exhibit an upper limit, and therefore, the corresponding excess-charge densities $N_{GB,charge}$ also feature an upper limit. The lower limit can be estimated to be 0.1 times the upper limit, in order to maintain about the same order of magnitude. The limits of the prefactor $s^n_{GB,0}$ have to be selected in a way that using the value ranges of $N_{GB,charge}$ and $s^n_{GB,0}$ in Eq. (13), the experimentally measured s_{GB} values are obtained (i.e., the $N_{GB,charge}$ and $s^n_{GB,0}$ value ranges remain the same for the complete s_{GB} datasets determined on the identical absorber material). We provide a full description of this approach at the examples of polycrystalline Cu(In,Ga)Se$_2$ and of multicrystalline Si wafers in Sec. III.

III. COMPARISON WITH EXPERIMENTAL RESULTS

The recombination velocity s_{GB} of a specific grain boundary in a polycrystalline semiconductor can be determined by evaluating cathodoluminescence (CL) intensity distributions across this planar defect. The corresponding procedure is described in Ref. 1. We provide an extensive description of this procedure also in Appendix B of the present work.

As shown in Sec. II, for a specific s_{GB} value, always, ranges of $N_{GB,charge}$ and $s^n_{GB,0}$ values can be determined. We will now apply this approach to experimentally measured s_{GB} values. (We note that in the evaluation procedure described in Ref. 1, the median value of all experimental s_{GB} values from a specific absorber is

22 June 2025 06:41:20

© Author(s) 2025

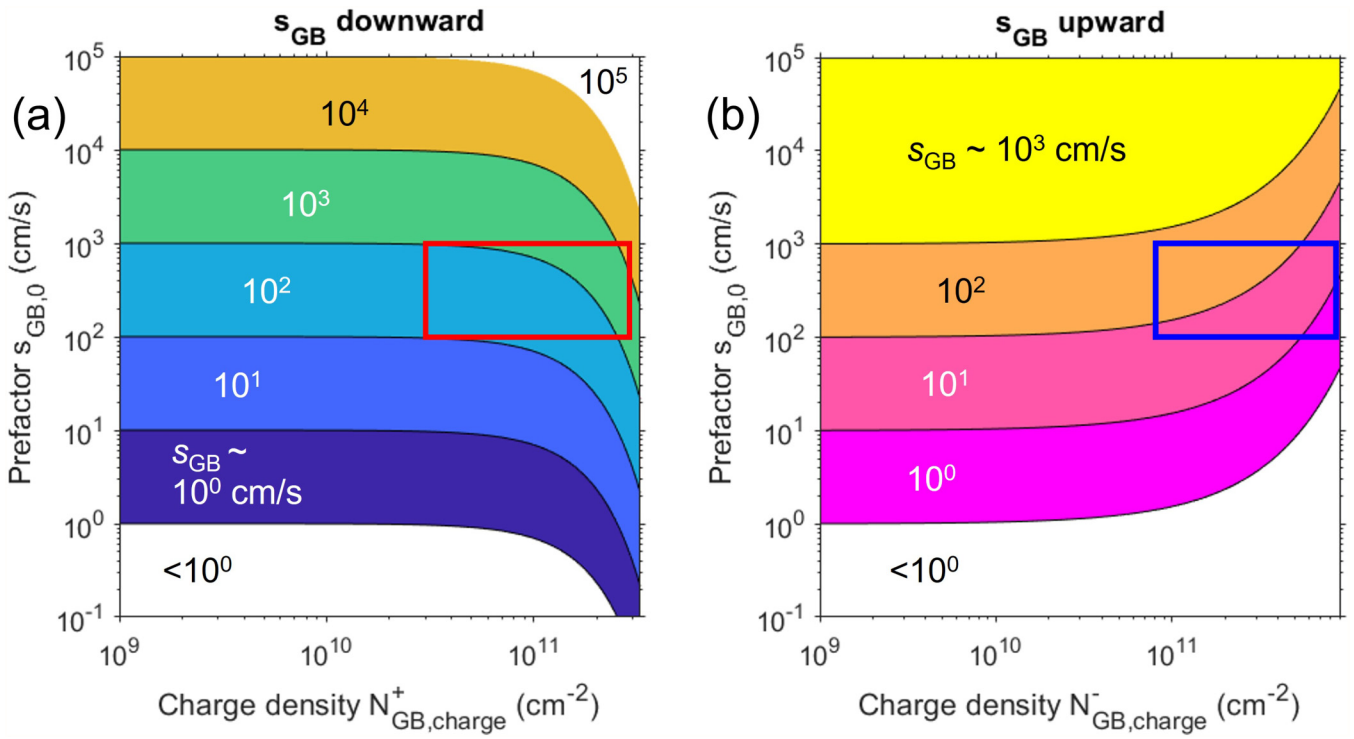

FIG. 4. The recombination velocity s_{GB} for (a) downward and (b) upward band bending as a function of the excess-charge density $N_{GB,charge}$ and of the prefactor $s^n_{GB,0}$, calculated using Eqs. (11)–(13) for $N_A = 2 \times 10^{16}$ cm^{-3}. Note that in subfigures (a) and (b), s_{GB} values are used as labels for regions with the same orders of magnitude. Highlighted by red (a) and blue (b) rectangles are the value ranges for the evaluation of the experimental s_{GB} data given in Fig. 5 (explained in detail in Sec. III).

22 June 2025 06:41:20

assumed to be the s_{GB} value for $\Phi_{GB} = 0$ eV, i.e., equal to the prefactor $s^n_{GB,0}$; however, we find that it is more appropriate to assume that $s^n_{GB,0}$ varies slightly between two grain boundaries in the same material, and thus, this approach was improved by the present work.)

Figure 5 provides the simulations of experimental s_{GB} values, ranging from about 20 to 5200 cm/s, which were determined by means of CL on a high-efficiency Cu(In,Ga)Se_2 layer[1,10] with

TABLE I. Ranges of the recombination velocity s_{GB} and the corresponding $N_{GB,charge}$ and $s_{GB,0}$ intervals, extracted from Figs. 4(a) and 4(b). Note that the excess-charge density represented by $N_{GB,charge}$ is positive for downward and negative for upward band bending.

Band-bending type	s_{GB} (cm/s)	$N_{GB,charge}$ (10^{11} cm^{-2})	$s^n_{GB,0}$ (cm/s)
Upward	1–2	0.01–9.1	1–100
Upward	10–20	0.01–9.1	10–1000
Upward	100–200	0.01–9.1	100–10 000
Downward	100–200	0.01–3.3	2–200
Downward	1000–2000	0.01–3.3	20–2000
Downward	10 000–20 000	0.01–3.3	200–20 000

$N_A = 2 \times 10^{16}$ cm^{-3}. We would like to remind that we assume similar (but not identical) defect properties at the corresponding grain boundaries and, therefore, determine the value ranges for $N_{GB,charge}$ and $s^n_{GB,0}$ that can be used to simulate successfully the experimental s_{GB} values; i.e., these $N_{GB,charge}$ and $s^n_{GB,0}$ value ranges are always the same for each s_{GB} dataset.

It is apparent from Figs. 4(a) and 4(b) that experimental s_{GB} values ranging over several orders of magnitude (i.e., 20–5200 cm/s) cannot be simulated assuming small $N_{GB,charge}$ values on the order of 10^9–10^{10} cm^{-2}. Therefore, the simulations shown in Fig. 5 are based on $N_{GB,charge}$ values restricted to $0.3 - 3$ (downward) and $0.9 - 9 \times 10^{11}$ cm^{-2} (upward band bending). For $s^n_{GB,0}$, a value range of 100–1000 cm/s, on the same order of magnitude as the median of the experimental s_{GB} values, 300 cm/s, was found to be appropriate. These intervals are highlighted in Figs. 4(a) and 4(b) by a red and a yellow rectangle.

The ranges of $N_{GB,charge}$ and $s^n_{GB,0}$ that result in the corresponding experimental s_{GB} values are given in Figs. 5(a) and 5(b). Figures 5(c) depicts the ranges for the band-bending values Φ_{GB}. It is apparent from Fig. 5 that several s_{GB} values can be modeled assuming both downward and upward band bending. The true excess-charge state of these grain boundaries (and, therefore, whether the band bending is upward or downward) cannot be revealed by the approach in the present work,

© Author(s) 2025

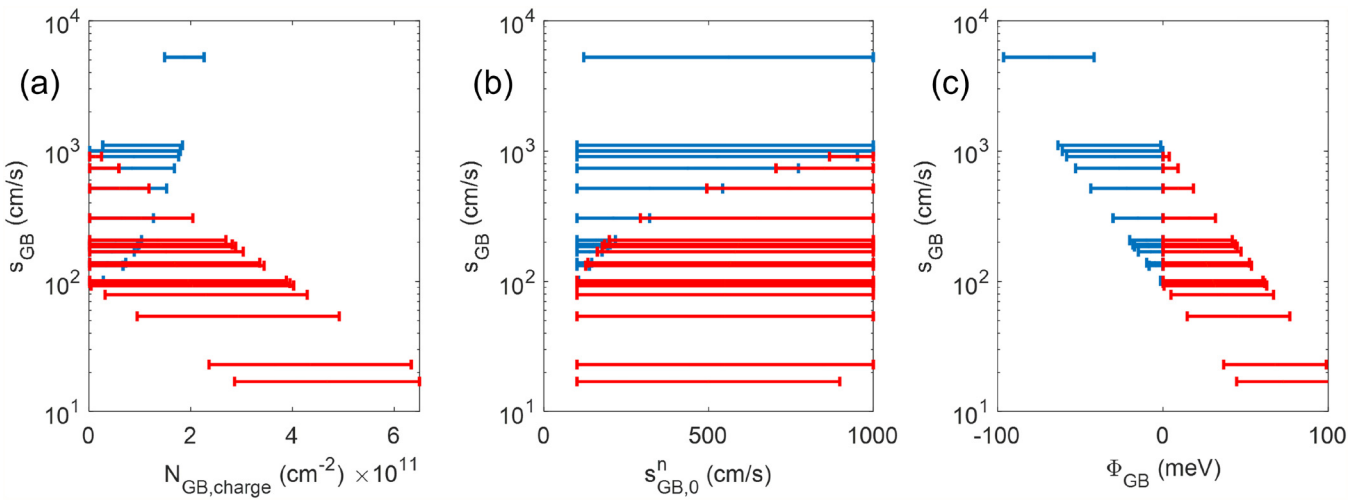

FIG. 5. Experimental s_{GB} values[1,10] as a function of (a) the defect density $N_{GB,charge}$, of the prefactor $s^n_{GB,0}$ (b), as well as of the band bending Φ_{GB} (c). $N_{GB,charge}$ was restricted to 0.3–3 (downward) and 0.9–9 × 10^{11} cm^{-2} (upward band bending), $s^n_{GB,0}$ to the interval of 100–1000 cm/s. The blue bars stand for downward band bending and the red ones for upward band bending.

but may be assessed by electrical analyses in scanning-probe microscopy, such as by conductive atomic force microscopy. Nevertheless, the ranges of $N_{GB,charge}$ and $s^n_{GB,0}$ (Fig. 5) can be used as input parameters in multidimensional device simulations.

In Appendix C1 and C2 (Figs. 7–9), evaluations of the s_{GB} values as the one shown in Fig. 5 are demonstrated for (Ag,Cu)(In,Ga)Se_2 and Si solar-cell absorbers. It is apparent that basically, the s_{GB} values for an individual absorber material always exhibit distributions over several orders of magnitude, and thus, the magnitudes as well as the distributions of $N_{GB,charge}$, $s^n_{GB,0}$, and Φ_{GB} are similar to those in Fig. 5. Overall, we simulated the experimental s_{GB} values from various multicrystalline Si, (Ag,Cu)(In,Ga)Se_2, CdTe, kesterite-type, and halide-perovskite absorbers successfully by always using $N_{GB,charge}$ and $s^n_{GB,0}$ ranges on the same orders of magnitude for a specific absorber (not all data shown in the present work). Thus, the presented approach is a general procedure to estimate the orders of magnitude of the effective defect density and its capture cross section for any photovoltaic absorber material.

IV. CORRELATION OF EXCESS CHARGES AND COMPOSITIONAL CHANGES AT GRAIN-BOUNDARY PLANES

In polycrystalline compound semiconductors, grain boundaries feature changes in composition within a very narrow range on the order of 0.1–1 nm. These changes have been interpreted as atomic/ionic reconstructions of the atomic planes adjacent to the grain boundary.[8,13] It is a valid question of whether different $N_{GB,charge}$ and $s^n_{GB,0}$ values, leading to substantiallly different recombination velocities s_{GB}, are related to different types of compositional changes found at different grain boundaries.[14,15]

In order to address this question, it makes sense to regard the orders of magnitude of the charge densities at the grain-boundary plane (that are screened by the free charge carriers) as well as those of the detected compositional changes. Since the $N_{GB,charge}$ values

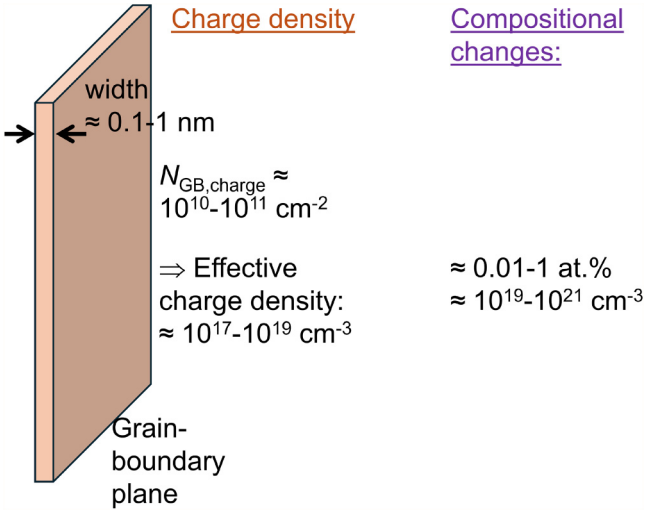

FIG. 6. Schematics of the charge density at a grain-boundary plane (left) and the magnitude of the compositional changes around this planar defect (right). From the considerations and results in the present work, the effective charge density can be assumed to be about 10^{17}–10^{19} cm^{-3}, while the compositional changes typically detected via various microscopic analysis tools reside on larger orders of magnitude (10^{19}–10^{21} cm^{-3}); thus, effects of the local composition on the charge density present at a specific grain boundary cannot be verified easily by the available analysis tools.

22 June 2025 06:41:20

© Author(s) 2025

were found to be on the order of 10^{10}–10^{11} cm^{-2}, and since the width of the grain boundary can be estimated to about 0.1–1 nm, the total charge density is about 10^{17}–10^{19} cm^{-3}. On the other hand side, the changes in composition, also including impurity atoms, are typically on the order of 0.01–1 at.%, i.e., about 10^{19}–10^{21} cm^{-3} (see also Fig. 6). Thus, the change in the charge density $N_{\mathrm{GB,charge}}$ at a grain boundary can be orders of magnitude smaller than the changes in composition that can easily be detected by available characterization techniques with suitable spatial resolution and sensitivity (e.g., atom-probe tomography); under ideal conditions, the total charge density and the chemical sensitivity of the analysis tool (referring to the detection of lateral *changes* in composition, not to the detection of impurities) may exhibit the same order of magnitude (10^{19} cm^{-3}). Nevertheless, in general, it is very difficult (if not impossible) to verify whether or not a direct correlation exists between changes in the charge density and changes in the composition.

V. CONCLUSIONS

The present work revisited the determination procedures and magnitudes of recombination velocities at grain boundaries. It was described that experimentally measured recombination velocities s_{GB} can be simulated using specific value pairs of the charged defect density $N_{\mathrm{GB,charge}}$ and of the prefactor $s^{n}_{\mathrm{GB},0}$. For one specific (experimental) s_{GB} value, always intervals of appropriate $N_{\mathrm{GB,charge}}$ and $s^{n}_{\mathrm{GB},0}$ values are found. However, for the experimentally measured s_{GB} values ranging from several 10^{0} to several 10^{4} cm/s, the intervals for $N_{\mathrm{GB,charge}}$ exhibit about the same orders of magnitude, about 10^{10}–10^{11} cm^{-2}, with resulting values for the prefactor $s_{\mathrm{GB},0}$ of about 10^{2}–10^{3} cm/s. Finally, it has been outlined that the compositional changes at the grain boundaries that may be linked to changes in charged defect densities leading to enhanced nonradiative recombination are so small that their detection is very difficult using the currently available analytical tools.

ACKNOWLEDGMENTS

The authors are grateful to Ulrike Bloeck (HZB) for assistance with the cross-sectional specimen preparation for SEM. The present work was supported by the German–Israeli Helmholtz International Research School HI-SCORE (HIRS-0008) and by the project "EFFCIS-II" funded by the Federal Ministry for Economic Affairs and Climate Action (BMWK) under Contract Nos. 03EE1059B (HZB) and 03EE1059C (MLU).

AUTHOR DECLARATIONS

Conflict of Interest

The authors have no conflicts to disclose.

Author Contributions

Daniel Abou-Ras: Conceptualization (equal); Writing – original draft (equal). **Matthias Maiberg:** Writing – original draft (equal).

DATA AVAILABILITY

The data that support the findings of this study are available from the corresponding author upon reasonable request.

APPENDIX A: DERIVATION OF BAND-BENDING VALUES AT GRAIN BOUNDARIES

1. Negative excess charge at a grain boundary

We assume a grain-boundary plane with negligible thickness and negative excess-charge density $N^{-}_{\mathrm{GB,charge}}$ at position x=0. At sufficiently high net-doping density in a p-type semiconductor, this excess charge will be screened by free holes ($x \geq 0$),

$$\rho(x) = qN_{\mathrm{A}}A\exp(-x/w), \tag{A1}$$

where q is the charge of a hole and w is the screening length (on both sides of the grain-boundary plane). Assuming a symmetrical distribution of $\rho(x)$ around $x = 0$, the following equation must hold:

$$\begin{gathered} \tfrac{1}{q}\int_0^{\infty}\rho(x)\mathrm{d}x = \frac{N^{-}_{\mathrm{GB,charge}}}{2} \\ \Leftrightarrow \tfrac{1}{q}\int_0^{\infty} qN_{\mathrm{A}}A\,\exp(-x/w)\,\mathrm{d}x = \frac{N^{-}_{\mathrm{GB,charge}}}{2} \\ \Leftrightarrow A = N^{-}_{\mathrm{GB,charge}}/(2wN_{\mathrm{A}}). \end{gathered} \tag{A2}$$

The electrical field is calculated via

$$F(x) = -qN_{\mathrm{A}}Aw/(\epsilon_0\epsilon_{\mathrm{r}})\exp(-x/w). \tag{A3}$$

Integration of $F(x)$ results in the electrostatic potential,

$$\phi(x) = -\frac{qN_{\mathrm{A}}Aw^2}{2\epsilon_0\epsilon_{\mathrm{r}}}\exp(-x/w). \tag{A4}$$

The hole density $p(x)$

$$p(x) = \rho(x)/q + N_{\mathrm{A}} = N_{\mathrm{A}}A\,\exp(-x/w) + N_{\mathrm{A}} \tag{A5}$$

must fulfill the continuity equation

$$\begin{gathered} \overrightarrow{\mathrm{div}}\,\vec{j}\,(x) - \frac{\mathrm{d}}{\mathrm{d}t}p(x) = 0 \\ \Leftrightarrow \frac{\mathrm{d}}{\mathrm{d}x}j(x) = q\frac{\mathrm{d}}{\mathrm{d}x}\left[\mu p(x)F(x) - D\frac{\mathrm{d}}{\mathrm{d}x}p(x)\right] = 0 \\ \Leftrightarrow p(x)F(x) - \frac{k_{\mathrm{B}}T}{q}\frac{\mathrm{d}}{\mathrm{d}x}p(x) = 0 \\ \Leftrightarrow -p(x)\frac{\mathrm{d}}{\mathrm{d}x}\phi(x) - \frac{k_{\mathrm{B}}T}{q}\frac{\mathrm{d}}{\mathrm{d}x}p(x) = 0 \end{gathered} \tag{A6}$$

22 June 2025 06:41:20

© Author(s) 2025

assuming a stationary case $[\frac{\mathrm{d}}{\mathrm{d}r}p(x)=0]$ and using Einstein's relationship $qD=\mu k_\mathrm{B}T$.

Applying Eqs. (A5) and (A4), Eq. (A6) becomes

$$\begin{aligned}&\left[N_\mathrm{A}A\exp\left(-\tfrac{x}{w}\right)+N_\mathrm{A}\right]\frac{qN_\mathrm{A}Aw}{\epsilon_0\epsilon_\mathrm{r}}\exp\left(-\frac{x}{w}\right)-\frac{k_\mathrm{B}T}{q}\frac{N_\mathrm{A}A}{w}\exp\left(-\frac{x}{w}\right)=0\\ &\Leftrightarrow N_\mathrm{A}A\exp\left(-\frac{x}{w}\right)\left[\left(A\exp\left(-\frac{x}{w}\right)+1\right)-\frac{k_\mathrm{B}T\epsilon_0\epsilon_\mathrm{r}}{q^2N_\mathrm{A}w^2}\right]=0\\ &\Leftrightarrow\frac{N^-_\mathrm{GB,charge}}{2wN_\mathrm{A}}\exp\left(-\frac{x}{w}\right)+1-\frac{k_\mathrm{B}T\epsilon_0\epsilon_\mathrm{r}}{q^2N_\mathrm{A}w^2}=0\end{aligned}\tag{A7}$$

using $A=N^-_\mathrm{GB,charge}/(2wN_\mathrm{A})$ [Eq. (A2)]. In the following, we consider the limit case of large N_A and small $N^-_\mathrm{GB,charge}$, i.e., $N_\mathrm{GB,charge}/(2wN_\mathrm{A})\exp(-x/w)\le N^-_\mathrm{GB,charge}/(2wN_\mathrm{A})\ll 1$; as outlined in the present work, this condition is fulfilled for various polycrystalline absorber materials. Thus, Eq. (A7) becomes

$$\begin{aligned}&1-\frac{k_\mathrm{B}T\epsilon_0\epsilon_\mathrm{r}}{q^2N_\mathrm{A}w^2}=0\\ &\Leftrightarrow w^2=\frac{k_\mathrm{B}T\epsilon_0\epsilon_\mathrm{r}}{q^2N_\mathrm{A}}\\ &\Leftrightarrow w=\sqrt{\frac{k_\mathrm{B}T\epsilon_0\epsilon_\mathrm{r}}{q^2N_\mathrm{A}}},\end{aligned}\tag{A8}$$

which is exactly the equation for the Debye screening length (see, e.g., Ref. 16). The amplitude A follows:

$$A=\frac{N^-_\mathrm{GB,charge}}{2wN_\mathrm{A}}=\frac{qN^-_\mathrm{GB,charge}}{2\sqrt{k_\mathrm{B}T\epsilon_0\epsilon_\mathrm{r}N_\mathrm{A}}}.\tag{A9}$$

We can use the equations for w and A [Eqs. (A8) and (A9)] to determine the electrostatic potential ϕ [Eq. (A4)] at position $x=0$,

$$\begin{aligned}\phi(x=0)&=-\frac{qN_\mathrm{A}}{2\epsilon_0\epsilon_\mathrm{r}}\frac{qN^-_\mathrm{GB,charge}}{2\sqrt{k_\mathrm{B}T\epsilon_0\epsilon_\mathrm{r}N_\mathrm{A}}}\frac{k_\mathrm{B}T\epsilon_0\epsilon_\mathrm{r}}{q^2N_\mathrm{A}}\\ &=-\frac{\sqrt{k_\mathrm{B}T}N^-_\mathrm{GB,charge}}{4\sqrt{\epsilon_0\epsilon_\mathrm{r}N_\mathrm{A}}}.\end{aligned}\tag{A10}$$

The upward band bending $\Phi^\mathrm{up}_\mathrm{GB}=-q\phi(x=0)$ results in

$$\Phi^\mathrm{up}_\mathrm{GB}=\frac{\sqrt{k_\mathrm{B}T}qN^-_\mathrm{GB,charge}}{4\sqrt{\epsilon_0\epsilon_\mathrm{r}N_\mathrm{A}}}.\tag{A11}$$

2. Positive excess charge at a grain boundary

We assume a grain-boundary plane with negligible thickness and positive excess-charge density $N^+_\mathrm{GB,charge}$ at position x=0. At sufficiently high net-doping density in a p-type semiconductor, this excess charge will be screened by ionized acceptors,

$$\rho(x)=-qN_\mathrm{A}.\tag{A12}$$

The electrical field is calculated via

$$F(x)=\frac{qN_\mathrm{A}(w+x)}{\epsilon_0\epsilon_\mathrm{r}}.\tag{A13}$$

Integration of $F(x)$ results in the electrostatic potential for $-w\le x\le w$,

$$\phi(x)=\frac{qN_\mathrm{A}(w+x)^2}{2\epsilon_0\epsilon_\mathrm{r}}.\tag{A14}$$

Using $N_\mathrm{A}=N^+_\mathrm{GB,charge}/(2w)$, the downward band bending $\Phi^\mathrm{down}_\mathrm{GB}=-q\phi(x=0)$ results in

$$\Phi^\mathrm{down}_\mathrm{GB}=-\frac{\left(qN^+_\mathrm{GB,charge}\right)^2}{8\epsilon_0\epsilon_\mathrm{r}N_\mathrm{A}}.\tag{A15}$$

APPENDIX B: DETERMINATION OF RECOMBINATION VELOCITIES s_GB AT GRAIN BOUNDARIES FROM CATHODOLUMINESCENCE INTENSITY DISTRIBUTIONS

The procedure of determining the recombination velocities s_GB at grain boundaries in a polycrystalline semiconductor material from cathodoluminescence (CL) analyses was first proposed by Mendis *et al.*[17] Linescans across grain boundaries (typically at least 15–20 for decent statistics) are extracted from CL intensity distributions, ideally acquired on polished cross sections in order to reduce roughnesses on the analyzed specimen areas, which may lead to artifacts of the measurements. The CL linescans exhibit local minima at the positions of the grain boundaries at $x=0$. For the determination of the recombination velocities s_GB, not the CL intensity difference between grain interiors and grain boundaries is evaluated; instead, the following equation is used:

$$\ln\left(1-\frac{I_\mathrm{CL}(x)}{I^\mathrm{GI}_\mathrm{CL}}\right)=\ln\left(\frac{S}{S+1}\right)-\frac{x}{L},\tag{B1}$$

where $I_\mathrm{CL}(x)$ and $I^\mathrm{GI}_\mathrm{CL}$ are the CL intensities along the linescan and in the grain interior, and S is the reduced recombination velocity expressed by

$$S=\frac{s_\mathrm{GB}\tau_\mathrm{bulk}}{L},\tag{B2}$$

22 June 2025 06:41:20

© Author(s) 2025

where τ_{bulk} is the bulk lifetime of the semiconductor material and L is the effective diffusion length of the minority-charge carriers. Equation (B1) represents a linear function, which can be fitted using L as a fit parameter and the coordinate x as a variable, which allows for extracting L from the slope and S from the intersect (for obvious reasons, $I_{CL}(x) = I_{CL}^{GI}$ needs to be avoided).

The challenging issue of this approach is the determination of the bulk lifetime τ_{bulk}, which is rather difficult to assess, in contrast to the effective lifetime τ_{eff} that can be extracted, e.g., from transients in time-resolved photoluminescence measurements. We can express the inverse of the effective lifetime for a bare, polycrystalline semiconductor material, including surface and grain boundaries via Matthiessen's rule,

$$\frac{1}{\tau_{eff}} = \frac{1}{\tau_{bulk,eff}} + \frac{1}{\tau_{GB}}, \tag{B3}$$

where $1/\tau_{bulk,eff} = 1/\tau_{bulk} + 1/\tau_{surf}$ and τ_{GB} is the average lifetime at the grain-boundary plane (τ_{surf} is the lifetime at the surface, and we assume that the lifetime of dislocations is included in the bulk lifetime).

After measuring τ_{eff}, $\tau_{bulk,eff}$ is estimated, which results in a value for τ_{GB} using Eq. (B3). We assume that during a CL experiment, the surface recombination and, thus, the surface lifetime τ_{surf} are the same at all coordinate values x; therefore, we set $\tau_{bulk,eff} = \tau_{bulk}$ in Eq. (B2). The measured CL linescans across grain boundaries are evaluated using Eq. (B1), with the estimated $\tau_{bulk,eff}$ used in Eq. (B2). From all s_{GB} determined, the median value $s_{GB,median}$ is calculated, from which another value of the average grain-boundary lifetime can be found via

$$\tau_{GB} = \frac{d_{grain}}{6 s_{GB,median}}, \tag{B4}$$

where d_{grain} is the average grain size measured, e.g., by electron backscatter diffraction. The described approach is now repeated iteratively until the grain-boundary lifetimes in Eqs. (B3) and (B4) are the same (not identical). We note that the same τ_{bulk} and τ_{GB} values have to be used for the determination of all the s_{GB} in a polycrystalline semiconductor material.

APPENDIX C: CASE STUDIES OF RECOMBINATION VELOCITIES AT GRAIN BOUNDARIES IN (Ag,Cu)(In,Ga)Se_2 AND MICROCRYSTALLINE Si SOLAR-CELL ABSORBERS

1. Case study I: Evaluation of recombination velocities at grain boundaries in (Ag,Cu)(In,Ga)Se_2 solar-cell absorbers

The following results (Figs. 7 and 8) were gathered on a Cu(In,Ga)Se_2 solar-cell absorber with a [Ga]/([Ga]+[In]) (GGI) ratio of 0.34 and on a (Ag,Cu)(In,Ga)Se_2 solar-cell absorber with an [Ag]/([Ag]+[Cu]) (AAC) ratio of 0.14. We note that the results shown below are not representative for (Ag,Cu)(In,Ga)Se_2 layers with similar GGI ratios.

2. Case study II: Evaluation of recombination velocities at grain boundaries in a wafer-based, microcrystalline Si solar-cell absorber

The s_{GB} values in the following viewgraph (Fig. 9) were extracted from Sio *et al.*,[9] who determined the recombination

22 June 2025 06:41:20

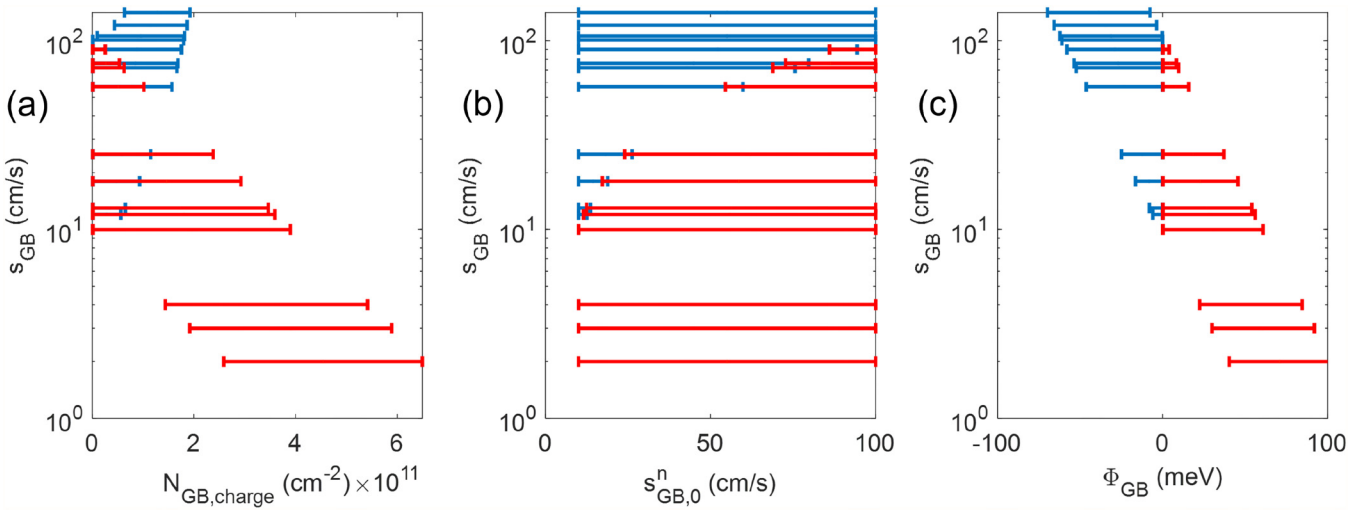

FIG. 7. Experimental s_{GB} values from a Cu(In,Ga)Se_2 layer with GGI = 0.34[11] as a function of (a) the defect density $N_{GB,charge}$, (b) of the prefactor $s^n_{GB,0}$, as well as (c) of the band bending Φ_{GB}. The net-doping density was $N_A = 1 \times 10^{16}$ cm^{-3}, while $N_{GB,charge}$ was restricted to 0.2–2 (downward) and 0.7–7 × 10^{11} cm^{-2} (upward band bending), $s^n_{GB,0}$ to the interval 10–100 cm/s (the median of the experimental s_{GB} values was about 30 cm/s). The blue bars stand for downward band bending and the red ones for upward band bending.

© Author(s) 2025

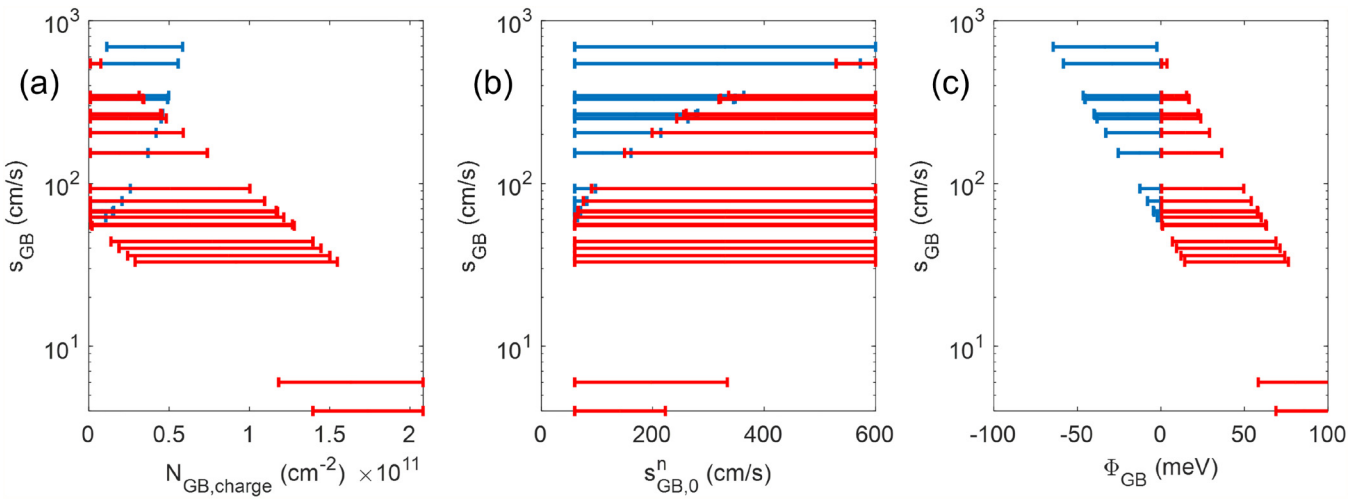

FIG. 8. s_{GB} values from a (Ag,Cu)(In,Ga)Se_2 layer with AAC = 0.14[12] as a function of (a) the defect density $N_{GB,charge}$, (b) of the prefactor $s^n_{GB,0}$, as well as (c) of the band bending Φ_{GB}. The net-doping density was $N_A = 1 \times 10^{15}$ cm^{-3}, while $N_{GB,charge}$ was restricted to 0.06–0.6 (downward) and 0.2–2 $\times$ 10^{11} cm^{-2} (upward band bending), $s^n_{GB,0}$ to the interval 60–600 cm/s (the median of the experimental s_{GB} values was about 100 cm/s). The blue bars stand for downward band bending and the red ones for upward band bending.

velocities at grain boundaries by means of photoluminescence imaging in multicrystalline Si wafers, which underwent various treatments (gettered, hydrogenated, as well as gettered and hydrogenated). An interesting fact from this work is that the treated Si wafers do not exhibit smaller s_{GB} values than the as-cut Si wafer. It is noted by Sio *et al.*[9] that the applied procedure cannot detect s_{GB} values of smaller than about 200 cm/s, which definitely has an impact on the magnitudes of the extracted $N_{GB,charge}$ and $s^n_{GB,0}$ values.

22 June 2025 06:41:20

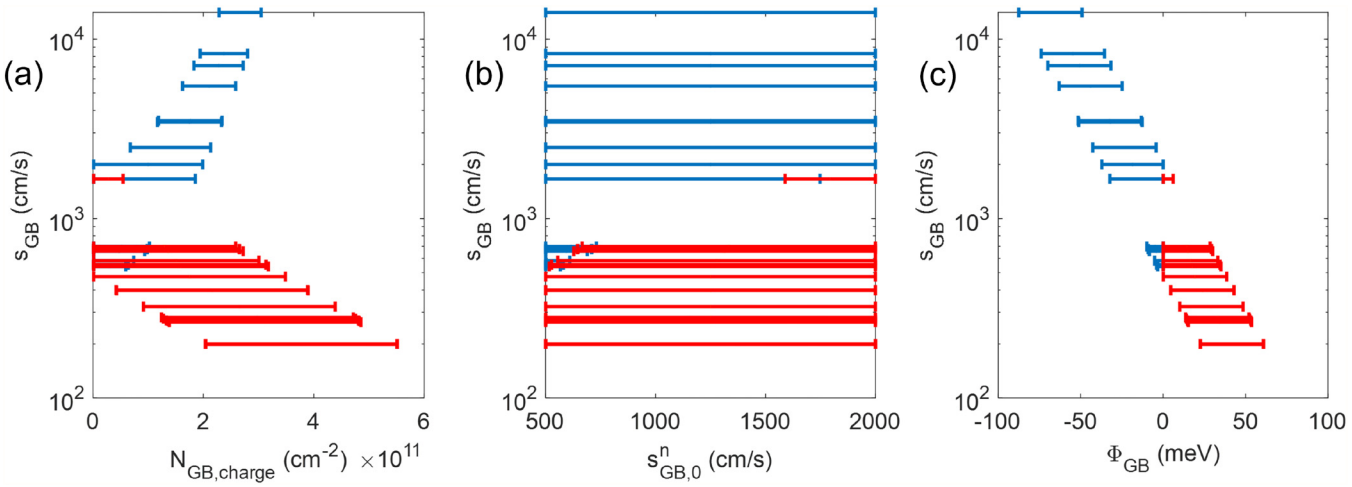

FIG. 9. s_{GB} values from a multicrystalline Si wafer (as-cut)[9] as a function of (a) the defect density $N_{GB,charge}$, (b) of the prefactor $s^n_{GB,0}$, as well as (c) of the band bending Φ_{GB}. The net-doping density was $N_A = 2 \times 10^{16}$ cm^{-3}, while $N_{GB,charge}$ was restricted to 0.2–2 (downward) and 0.7–7 $\times$ 10^{11} cm^{-2} (upward band bending), $s^n_{GB,0}$ to the interval 200–2000 cm/s (the median of the experimental s_{GB} values was about 1000 cm/s). The blue bars stand for downward band bending and the red ones for upward band bending.

© Author(s) 2025

REFERENCES

[1]J. Quirk, M. Rothmann, W. Li, D. Abou-Ras, and K. P. McKenna, Appl. Phys. Rev. **11**, 011308 (2024).
[2]J. Y. W. Seto, J. Appl. Phys. **46**, 5247 (1975).
[3]A. G. Aberle, Prog. Photovolt.: Res. Appl. **8**, 473 (2000).
[4]J. Brody and A. Rohatgi, Solid-State Electron. **45**, 1549 (2001).
[5]H. Neumann and R. Tomlinson, Sol. Cells **28**, 301 (1990).
[6]B. E. McCandless, W. A. Buchanan, C. P. Thompson, G. Sriramagiri, R. J. Lovelett, J. Duenow, D. Albin, S. Jensen, E. Colegrove, J. Moseley, H. Moutinho, S. Harvey, M. Al-Jassim, and W. K. Metzger, Sci. Rep. **8**, 14519 (2018).
[7]M. A. Scarpulla, B. McCandless, A. B. Phillips, Y. Yan, M. J. Heben, C. Wolden, G. Xiong, W. K. Metzger, D. Mao, D. Krasikov, I. Sankin, S. Grover, A. Munshi, W. Sampath, J. R. Sites, A. Bothwell, D. Albin, M. O. Reese, A. Romeo, M. Nardone, R. Klie, J. M. Walls, T. Fiducia, A. Abbas, and S. M. Hayes, Sol. Energy Mater. Sol. Cells **255**, 112289 (2023).
[8]D. Abou-Ras, B. Schaffer, M. Schaffer, S. S. Schmidt, R. Caballero, and T. Unold, Phys. Rev. Lett. **108**, 075502 (2012).
[9]H. Sio and D. Macdonald, Sol. Energy Mater. Sol. Cells **144**, 339 (2016).
[10]M. Krause, A. Nikolaeva, M. Maiberg, P. Jackson, D. Hariskos, W. Witte, J. A. Márquez, S. Levcenko, T. Unold, R. Scheer, and D. Abou-Ras, Nat. Commun. **11**, 4189 (2020).
[11]S. Thomas, W. Witte, D. Hariskos, S. Paetel, C. Song, H. Kempa, M. Maiberg, N. El-Ganainy, and D. Abou-Ras, Prog. Photovolt.: Res. Appl. **33**, 265 (2025).
[12]S. Thomas, W. Witte, D. Hariskos, R. Gutzler, S. Paetel, C. Song, H. Kempa, M. Maiberg, and D. Abou-Ras, Prog. Photovolt.: Res. Appl. **32**, 930 (2024).
[13]D. Abou-Ras, S. S. Schmidt, R. Caballero, T. Unold, H. Schock, C. T. Koch, B. Schaffer, M. Schaffer, P. Choi, and O. Cojocaru-Mirédin, Adv. Energy Mater. **2**, 992 (2012).
[14]D. Abou-Ras, S. S. Schmidt, N. Schäfer, J. Kavalakkatt, T. Rissom, T. Unold, R. Mainz, A. Weber, T. Kirchartz, E. S. Sanli, P. A. van Aken, Q. M. Ramasse, H. Kleebe, D. Azulay, I. Balberg, O. Millo, O. Cojocaru-Mirédin, D. Barragan-Yani, K. Albe, J. Haarstrich, and C. Ronning, Phys. Status Solidi (RRL) **10**, 363 (2016).
[15]O. Cojocaru-Mirédin, T. Schwarz, and D. Abou-Ras, Scr. Mater. **148**, 106 (2018).
[16]S. Sze and K. K. Ng, *Physics of Semiconductor Devices* (Wiley, 2006).
[17]B. G. Mendis, L. Bowen, and Q. Z. Jiang, Appl. Phys. Lett. **97**, 092112 (2010).

22 June 2025 06:41:20

© Author(s) 2025